Nuclear Instruments and Methods in Physics Research A 654 (2011) 399–405

Contents lists available at ScienceDirect

Nuclear Instruments and Methods in Physics Research A

journal homepage: www.elsevier.com/locate/nima

Measurement of the neutron fields produced by a 62 MeV proton beam on a PMMA phantom using extended range Bonner sphere spectrometers

K. Amgarou [a], R. Bedogni [b,*], C. Domingo [a], A. Esposito [b], A. Gentile [b], G. Carinci [b], S. Russo [c]

[a] Grup de Recerca en Radiacions Ionitzants, Departament de Física, Universitat Autònoma de Barcelona, E-08193 Bellaterra, Spain
[b] INFN—Istituto Nazionale di Fisica Nucleare, Laboratori Nazionali di Frascati, Via E. Fermi n. 40, 00044 Frascati, Italy
[c] INFN—Istituto Nazionale di Fisica Nucleare, Laboratori Nazionali del Sud, via S. Sofia 44, 95123 Catania, Italy

ARTICLE INFO

Article history:
Received 18 June 2011
Received in revised form
14 July 2011
Accepted 16 July 2011
Available online 26 July 2011

Keywords:
Proton therapy beam
Secondary radiation
Neutron spectrometry
Bonner spheres

ABSTRACT

The experimental characterization of the neutron fields produced as parasitic effect in medical accelerators is assuming an increased importance for either the patient protection or the facility design aspects. Medical accelerators are diverse in terms of particle type (electrons or hadrons) and energy, but the radiation fields around them have in common (provided that a given threshold energy is reached) the presence of neutrons with energy span over several orders of magnitude. Due to the large variability of neutron energy, field or dosimetry measurements in these workplaces are very complex, and in general, cannot be performed with ready-to-use commercial instruments.

In spite of its poor energy resolution, the Bonner Sphere Spectrometer (BSS) is the only instrument able to simultaneously determine all spectral components in such workplaces. The energy range of this instrument is limited to $E < 20$ MeV if only polyethylene spheres are used, but can be extended to hundreds of MeV by including metal-loaded spheres (extended range BSS, indicated with ERBSS).

With the aim of providing useful data to the scientific community involved in neutron measurements at hadron therapy facilities, an ERBSS experiment was carried out at the Centro di AdroTerapia e Applicazioni Nucleari Avanzate (CATANA) of INFN—LNS (Laboratori Nazionali del Sud), where a proton beam routinely used for ophthalmic cancer treatments is available. The 62 MeV beam was directed towards a PMMA phantom, simulating the patient, and two neutron measurement points were established at 0° and 90° with respect to the beam-line. Here the ERBSS of UAB (Universidad Autónoma de Barcelona—*Grup de Física de les Radiacions*) and INFN (Istituto Nazionale di Fisica Nucleare—Laboratori Nazionali di Frascati) were exposed to characterize the "forward" and "sideward" proton-induced neutron fields. The use of two ERBSS characterized by different set of spheres, central detectors, and independently established and calibrated, is important for guaranteeing the robustness of the measured spectra and estimating their overall uncertainties.

1. Introduction

Parasitic neutron fields are of practical importance for both electron (for energy higher than 10 MeV) and hadron medical accelerators. From the point of view of the occupation radiation protection, the neutron component must be carefully considered when designing lateral shields, ducts, doors, and labyrinths. In addition, dosemeters with adequate neutron response must be adopted for the surveillance of areas and personnel. From the point of view of the patient protection, the exposure to neutrons is a major concern, because the in-room neutron field produces a whole-body exposure of the patient, while the clinical beam selectively irradiates the treatment volume. As a consequence, the risk of long-term secondary cancer due to neutrons may be higher than that associated to the clinical beam and its scattered components [1,2].

Experimental studies evidenced that values of ambient dose equivalent ranging from about 0.1 to 1 mSv per prescribed Gy at the isocenter may be found in treatment rooms of medical electron LINACs, mainly depending on the field size and electron energy [3]. Larger values, up to about 20 mSv/Gy, can be observed in passively scattered proton-therapy units using large treatment fields [4].

For proton energies relevant to the medical field, i.e. below 250 MeV, the main neutron producing mechanisms are the (p,n) reactions in the accelerator materials and in the patient. The carbon is responsible for most of the neutron emission in tissue-like materials. The (p,n) reaction in carbon is characterized by a threshold (approximately. 13 MeV) and the neutron yield approximately increases as E_p^2 (E_p = proton energy) in the mentioned energy range [5].

* Corresponding author. Tel.: +39 0694032608; fax: +39 0694032364.
E-mail address: roberto.bedogni@lnf.infn.it (R. Bedogni).

0168-9002/$ - see front matter © 2011 Elsevier B.V. All rights reserved.
doi:10.1016/j.nima.2011.07.027

Neutrons are preferably produced in the MeV region, but all energies up to approximately the incident proton energy are possible. In addition, due to the scattering with surrounding materials, a substantial fraction of neutrons may be slowed down to thermal energies.

Due to the large variability of neutron energy, field or dosimetry measurements in these workplaces are very complex, and in general, cannot be performed with ready-to-use commercial instruments.

To date, only the Bonner Sphere Spectrometer (BSS) [6] is able to measure the neutron spectra, independently on their direction of incidence, over this large energy range [7]. This spectrometer consists of a set of polyethylene spherical moderators of various sizes surrounding a central detector mainly sensitive to thermal neutrons. As the size of the sphere increases, the maximum response of the sphere–detector combination shifts to higher energies. To accurately derive the thermal neutron component, the smallest spheres are frequently exposed with and without a Cd filter (typical thickness of 1 mm) [8]. A known limitation of the BSS is the poor energy resolution, due to the shape of the response functions that are characterized by similarities and overlapping. Particularly, the best energy resolution is in the interval between 0.1 and 20 MeV, corresponding to the maximum degree of differentiation of the response functions whereas poor resolution is found in the intermediate energy region ($0.5\ \text{eV} < E < 0.1\ \text{MeV}$) and above 20 MeV [9], where all response functions tend to have similar slopes. As a general rule, neutron spectra having a smooth and continuous shape can be well described by a BSS, while the fluence associated with narrow peaks or fine structures will be spread over a larger energy interval.

The use of pure polyethylene spheres has an inherent upper limit of application around 20 MeV, since the cross-section of the n–p elastic scatterings quickly drops above this energy [10]. In fact, increasing the diameter of the polyethylene sphere to more than about 30 cm (12 in.) has practically no effect on the response above 20 MeV. To extend the energy range of the BSS up to hundreds of MeV, layers of high Z materials such as lead, iron or copper have been embedded in the large spheres (usually 7 in. and higher) [11]. Neutrons above 20 MeV undergo inelastic reactions in these materials, thus resulting in low-energy secondary neutrons having a higher probability to interact in the central detector.

The UAB and INFN groups collaborated since 2003 in the research area of neutron dosimetry and spectrometry. Each group has independently established and validated its own ERBSS on the basis of different central detectors and set of spheres [12–16]. A series of experimental comparisons have been performed to compare the two systems, which provided the same results over a number of workplaces, ranging from quasi-mono-energetic neutron fields [17,18] to the neutron field generated around the high-energy DAΦNE electron-positron collider [19]. This collaboration allowed developing the FRUIT unfolding code [20,21]. This code is specially designed to derive the neutron spectra in environments where detailed pre-information is not available.

Whilst a number of works describing neutron spectrum measurements at carbon ion facilities are available in literature [22,23], few works on neutrons in proton-therapy facilities have been written, and most of them only include numerical simulations [4].

With the aim of providing useful data to the scientific community involved in neutron measurements at hadro-therapy facilities, an experimental campaign was organized at the Centro di AdroTerapia e Applicazioni Nucleari Avanzate (CATANA) of INFN—LNS (Laboratori Nazionali del Sud), where a proton beam routinely used for ophthalmic cancer treatments is available. The 62 MeV beam was directed towards a polymethylmethacrylate (PMMA) phantom, simulating the patient, and two neutron measurement points were established at 0° and 90° with respect to the beam-line. Here the ERBSS of UAB and INFN were exposed to characterize the "forward" and "sideward" proton-induced neutron fields. The use of two inter-validated ERBSS in the same measurement points is important for guaranteeing the robustness of the measured spectra and for a better estimation of uncertainties.

After a brief description of the two ERBSS and of the FRUIT unfolding code, this paper focuses on the analysis of the measured spectra. In addition, the paper reports the results of Monte Carlo simulations, carried out in a very simplified geometry, aimed at identifying the energy regions where the majority of the neutron production is expected.

2. The CATANA center at INFN-LNS (Catania, Italy)

The CATANA hadron therapy facility at INFN—LNS (Laboratori Nazionali del Sud) is in operation since 2002. Here a proton beam is used to treat shallow ocular tumors such as choroidal melanoma, cancer of the iris, screen-blastoma, and age-related macular degeneration [24,25]. The proton beam is extracted from a superconducting cyclotron and can be transported into several different experimental halls including the proton therapy room where a remote passive in-air dose delivery system has been assembled together with a dedicated positioning accessory for the patient immobilization. The adjustment of the beam field geometry to the irregular shape of the cancer subjected to healing as well as the control of the prescribed clinical dose that must be delivered to its respective malignant cells is assured by means of several components such as scattering foils, a set of transmission chambers, an on-line control planar ionization chamber detector, and specific collimators. The system normally uses a range-shifter multi-slab device and a rotating range-modulator wheel, both made of PMMA, to spread-out longitudinally the Bragg peak in depth, along the tumor inner volume.

3. Materials and methods

3.1. The UAB and INFN spectrometers

The INFN BSS [12–14] consists of 7 pure polyethylene (PE) spheres, whose diameters are labelled in inch units (2, 3, 5, 7, 8, 10, and 12 in.) for convenience, plus three high-energy spheres, called ERS-1, ERS-2, and ERS-3 and composed as follows:

LNF-ERS-1: external diameter 7 in. includes an internal 4 in. PE sphere surrounded by 1.27 cm of lead.
LNF-ERS-2: external diameter 7 in. includes an internal 4 in. PE sphere surrounded by 1.27 cm of copper.
LNF-ERS-3: external diameter 12 in. includes an internal 3.15 in. PE sphere surrounded by 1 cm of lead.

The central thermal neutron detector is a cylindrical $4\ \text{mm} \times 4\ \text{mm}$ ^{6}LiI(Eu). The response matrix, calculated with MCNPX version 2.4.0 [26] for 120 logarithmic equidistant discrete energy values between 1.5E−9 MeV and 1.16 GeV, was validated in radionuclide [27] or quasi-mono-energetic neutron reference fields [18]. Its overall uncertainty, found to be $\pm 3\%$, was estimated on the basis of these irradiations as the relative standard deviation of the ratio between the measured counts and those expected by folding the response matrix with the tabulated spectra. The calibration factor of this ERBSS is verified every 2 years by exposing the large spheres (5 in. and larger) to an NPL-calibrated ^{241}Am–Be source (the source strength is known within less than $\pm 1\%$). As a routine quality assurance program,

the efficiency of the central ^{6}LiI(Eu) detector is checked before and after any experimental campaign using a fixed-geometry portable moderator with a small (0.1 Ci) ^{241}Am–Be source in its center. As a result, the spectrometer calibration factor is known within less than $\pm 2\%$ uncertainty.

The UAB BSS is based on a cylindrical (10 mm diameter and 9 mm high) ^{3}He filled (8 kPa) proportional counter (model 05NH1 from EURISYS), 8 polyethylene (100% purity and 0.920 ± 0.003 g cm^{-3} density) spheres (2.5, 3, 4.2, 5, 6, 8, 10, and 12 in.) and a 1 mm thick cadmium (Cd) cover, which may be used for the 3 smallest spheres. The two extended range spheres, called UAB-ERS-1 and UAB-ERS-2, are composed as follows:

UAB-ERS-1: external diameter 7 in. includes an internal 4 in. PE sphere surrounded by 2.54 cm of lead.
UAB-ERS-2: external diameter 7 in. includes an internal 4 in. PE sphere surrounded by 2.54 cm of copper.

The response matrix of the UAB BSS was calculated, using MCNPX versions 2.4.0, for 121 logarithmic equidistant discrete energy values ranging from 7.943E−10 MeV up to 1.259 GeV. The matrix was validated in reference quasi mono-energetic beams at PTB (Braunschweig, Germany), as well as in radionuclide based sources and the thermal SIGMA facility at IRSN (Cadarache, France), providing an overall uncertainty of $\pm 3\%$.

The spectrometer was re-calibrated in March 2008 in the reference ^{241}Am–Be field of INFN and its calibration factor was confirmed within $\pm 2\%$.

3.2. The FRUIT unfolding code

The topic of neutron spectra unfolding for BSS has been widely treated already [28], and a number of unfolding codes have been developed, based on diverse mathematical procedures [29]. The main difficulty in unfolding BSS data arises from the fact that the number of measurements is lower (typically of an order of magnitude) than the number of energy bins used to represent the neutron spectrum. In addition BSS data cannot be considered as truely independent because the response functions of the spheres are normally continuous curves, characterized by overlapping and similarities. The BSS data must be complemented with a certain amount of *a priori* information. This can be done in two ways:

(a) By providing a *guess* spectrum, typically derived from Monte Carlo simulations and preferably very similar to the spectrum to be determined.
(b) By modeling the neutron spectrum as a superposition of elementary functions, covering the different energy domains and fully described by a reduced number (less than ten) of physically meaningful parameters. This approach, called *parametric*, is used in FRUIT and in the Bayesian methods [29].

The FRUIT code was especially designed as a tool for operational measurements in scenarios where very less pre information is available. Besides the sphere response functions, the counts and related uncertainties, FRUIT only requires to introduce qualitative information on the type of "radiation environment" on the basis of a check-box input section. The code randomly generates a default spectrum needed to start the iterative procedure, on the basis of the radiation environment selected by the user. Taking advantage of a "flexible tolerance" convergence mechanism, results do not depend on the numerical values of this spectrum. Other relevant aspects are as follows:

(1) The user intervenes to control the convergence procedure. The code is not intended as a "black box".
(2) User friendliness and visual operation. The quantities involved in the unfolding process and their variation are continuously displayed: the plot of the spectrum, the measured and unfolded Bonner sphere counts, the parameters, the tolerances, and the dosimetric quantities.
(3) The code includes a statistics tool deriving the probability distributions of all quantities related to the final spectrum: the parameters, the fluence (and fractions of fluence in given energy intervals), the ambient dose equivalent and the numerical values of the neutron spectrum, specified bin by bin. Uncertainties are derived by considering the 16–84% cumulative probability of these distributions. Uncertainties of input quantities (sphere counts, response matrix and other sources that may randomly affect the sphere counts) are used to perform these analyses.

The parametric approach may be very convenient in a variety of operational scenarios, especially if detailed a priori information is not available. By contrast, when the final spectrum is likely to be obtained by slightly perturbing a highly reliable "default" spectrum, the traditional "pure mathematical" convergence methods may be used with accurate results. For this purpose the FRUIT code, as an alternative to the parametric approach, includes an unfolding option that perturbs a default spectrum according to a special gradient method (SGM) [28].

It this work both parametric and SGM algorithms have been employed.

3.3. Experiment

The measurements were carried out at the INFN-LNS superconducting cyclotron complex, in a room called "sala 0°". Here the 62 MeV proton beam was sent on a $12 \times 12 \times 12$ cm^3 PMMA phantom whose center was located in the same plane as the proton beam axis. The proton beam had circular profile with diameter 2 mm and the nominal current was about 3.6 nA (as measured by the last current monitor before beam delivering). The position of points A and B were 110 cm in the forward direction and 190 cm in the sideward direction, respectively, with respect to the Bragg peak in the PMMA phantom (see Fig. 1). The distance between point A and the nearest wall is 50 cm.

Both ERBSS were exposed in both points A and B. For each measurement point, the spheres were sequentially exposed. Due

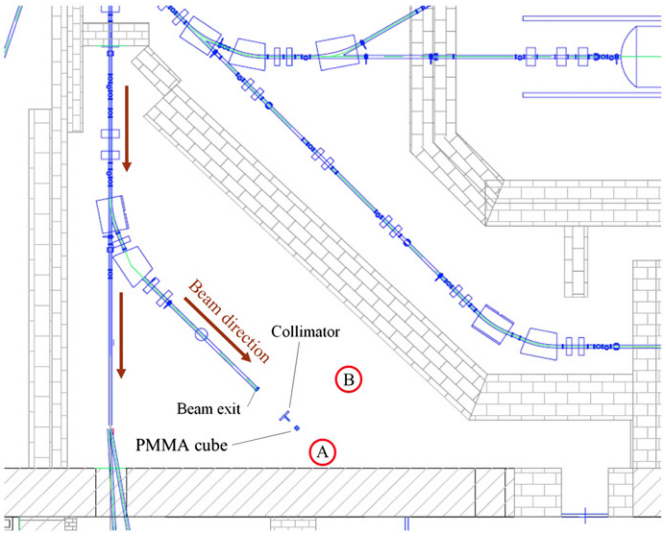

Fig. 1. Plan view of the experimental room at INFN-LNS with indication of the measurement points.

to the limited beam-time assigned to the campaign, the irradiation time was about 2.5 min./sphere. This was enough to guarantee statistical uncertainties lower than $\pm 0.6\%$. Because the time variability of the proton current was not negligible ($< \pm 8\%$), two monitor instruments, working in parallel with the ERBSS, were used to normalize the sphere readings. These were a Thermo FHT 62 rem-counter for the INFN system, and an additional 05NH1 Helium-3 proportional counter in a 4.2 in. polyethylene sphere for UAB. The monitor instruments were calibrated in terms of reading (μSv for the rem-counter, counts for the Helium-3 counter) per proton exciting the beam-line, obtaining the following factors: $f_{INFN}=(203\pm10)E-13$ μSv and $f_{UAB}=(1772\pm89)E-11$, respectively. The coherence between the two monitoring systems was checked by measuring their ratio in different time intervals. This value was found to be constant within $\pm 3\%$ (regarded as monitoring uncertainty).

For each ERBSS and each measurement point, the BSS counts were divided by the corresponding number of monitor units. The result (normalized BSS counts) was used as the input data for the unfolding procedures. Because the uncertainties on the BSS data are of great importance in the unfolding process, it is worth mentioning that the uncertainties of the normalized BSS counts (less than $\pm 5\%$) were obtained by a quadratic combination of the following: counting uncertainties (lower than $\pm 0.6\%$), by making response matrix of overall uncertainty ($\pm 3\%$), and monitoring uncertainty ($\pm 3\%$).

4. Monte Carlo simulations

The Monte Carlo code MCNPX version 2.4.0 was used in this work. Due to the impossibility to obtain very detailed information about the geometry and the materials composing the beam-line and the irradiation room, a simplified Monte Carlo model was assembled with the objective of identifying the energy regions where the main structures in the neutron spectrum could arise. Therefore a point-wise mono-energetic proton beam was supposed to impinge the PMMA cube. The inner space of the experimental hall was filled with dry air whereas its lateral walls, floor and ceiling were assumed to be made by 50 cm of ordinary concrete (density 2.35 g cm^{-3}).

All secondary particles such as neutrons, photons, and light ions (^{2}H, ^{3}H, ^{3}He, and ^{4}He), were transported in the PMMA cube. Concerning the interaction of primary protons with PMMA (composition $(C_5O_2H_8)_n$), the code implements tabulated cross-sections (LA150H library) up to 150 MeV.

Light ions may trigger further nuclear interactions able to generate extra neutrons. The mix and match control of the cross-section library data and physical models was enabled. For particles or energies not covered by the tabulated cross-sections, the BERTINI high-energy interaction model was selected to describe the following stages of the nuclear inelastic interactions: fast intra-nuclear cascade, pre-equilibrium decay, and de-excitation of residual nuclei.

The energy distribution of the neutron fluence in points A and B was obtained by means of point detectors (F5). No variance reduction techniques were employed and the number of histories was large enough to have relative statistical uncertainties $< \pm 2\%$ for all energy bins.

5. Results and discussion

Figs. 2 and 3 give a lethargy plot of the simulated neutron spectra, in points A and B normalized to the total fluence (unit spectra). The same plot include the response functions of the INFN and UAB spectrometers in order to shown the convenience of an extended range spectrometer to measure neutron spectra including energy components above 10 MeV. As already explained in Section 4, the simulations are not intended to exactly predict the neutron spectra in the measurement points, but should give an idea of the main structures that could arise in the spectra. This information is relevant for choosing the adequate spectrum parameterization in FRUIT. As expected, the simulated neutron spectra present the following components:

(1) A thermal peak, mainly due to the scattering of neutron in the phantom, in the air and in the room walls and structures.
(2) A fast neutron peak, due to the nuclear interactions of incident protons with the materials of the phantom (mainly carbon). The high-energy component ($E > 10$ MeV) is higher in the forward direction because high-energy neutrons from inelastic interactions of protons in the PMMA are forward peaked. In fact, the peak in the 0° spectrum arises at about 10 MeV. By contrast, the sideward spectrum has a peak at 3–4 MeV.
(3) A continuous intermediate spectrum.

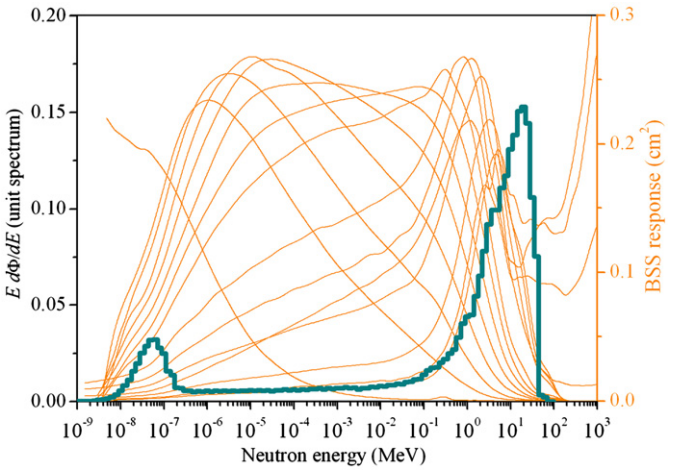

Fig. 2. Point A: MCNPX simulated spectrum superposed to the response functions of the INFN extended range Bonner sphere spectrometer. The spectrum is normalized to the unit fluence (unit spectrum) and in equi-lethargy representation.

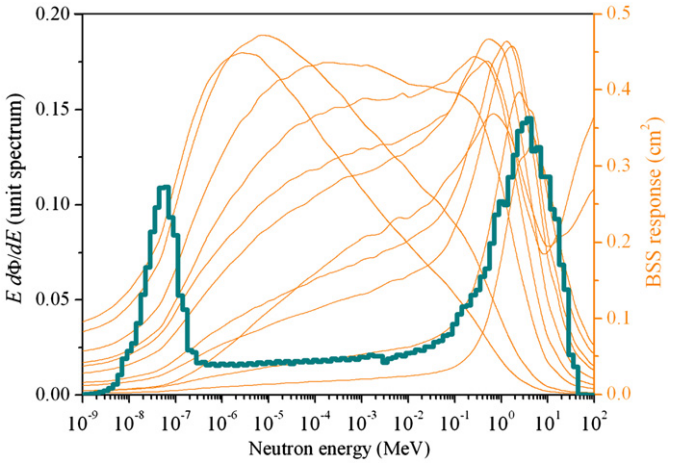

Fig. 3. Point B: MCNPX simulated spectrum superposed to the response functions of the UAB extended range Bonner sphere spectrometer. The spectrum is normalized to the unit fluence (unit spectrum) and in equi-lethargy representation.

The experimental data were unfolded with FRUIT, adopting the following parameterization [20]:

$$\varphi(E) = P_t\varphi_t(E) + P_e\varphi_e(E) + P_f\varphi_t(E) \quad (1)$$

where $\varphi(E)$ is the neutron spectrum normalized to unit integral (unit spectrum), P_t, P_e, and P_f are the weights of the thermal, epithermal, and fast component ($P_t+P_e+P_f=1$), respectively, $\varphi_t(E)$, $\varphi_e(E)$, and $\varphi_f(E)$ are the elementary functions (normalized to unit integral) describing the thermal, epithermal and fast components, respectively.

For the purposes of this work, it is important to say that the following formulation was chosen for $\varphi_f(E)$:

$$\varphi_f(E) = AE^{\alpha}\exp(-E/\beta) \quad (2)$$

where A is a normalization factor. α and β are positive numbers on whose basis the peak of the fast neutron component (in lethargy representation) may be located:

$$E_{peak} = \beta(\alpha+1). \quad (3)$$

Because this parameterization has been mainly used in FRUIT for unfolding low-energy data (e.g. nuclear plants, and medical accelerators), and its ability to describe a peak in the 10 MeV region (as expected in the forward direction) must be proved. For this reason the BSS counts obtained in point A were unfolded using both parametric and SGM options of FRUIT.

Fig. 4 shows the results of the SGM unfolding for UAB and INFN systems at point A. The spectrum derived with MCNPX was used as pre-information. Three are the main aspects of this plot:

(1) The UAB and INFN spectra coincide within the uncertainties. This confirms the high degree of coherence of these spectrometers.
(2) Both spectra show a complex peak in the 10 MeV region, as expected from the simulation.
(3) The uncertainties are large in high energy region, thus confirming the limitations of the ERBSS in this domain [9,30].

The same data were then unfolded using the parametric approach, which does not use default spectrum. The parametric and SGM spectra at point A are compared in Figs. 5 and 6 for UAB and INFN systems. The single peak, describing the fast neutron component in the parametric spectrum well agrees with the complex peak from the SGM approach, in terms of both peak location and shape of the high-energy component ($E > 10$ MeV). The differences observed in the 100 keV–10 MeV region are in practice comparable with the uncertainties. Differences in the epithermal domain can be ascribed to the poor resolving power of the ERBSS in this region [9].

For the point at 90° (point B) only the parametric approach was used, because the location of the peak (~MeV) is included in the region where this approach is known to work reliably [10].

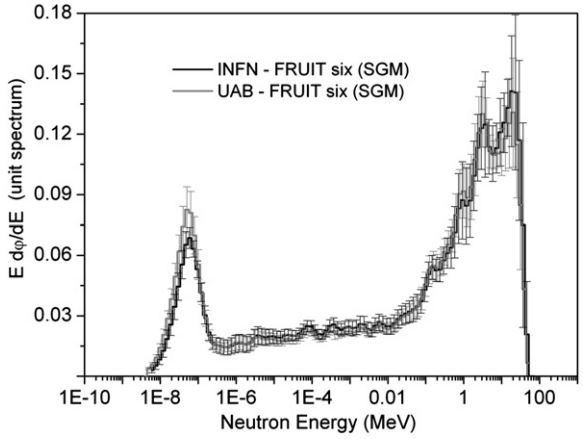

Fig. 4. Point A: neutron spectra unfolded with FRUIT ver. six using the SGM approach and the MCNPX simulated spectrum as default spectrum. The spectra are normalized to the unit fluence (unit spectra) and in equi-lethargy representation.

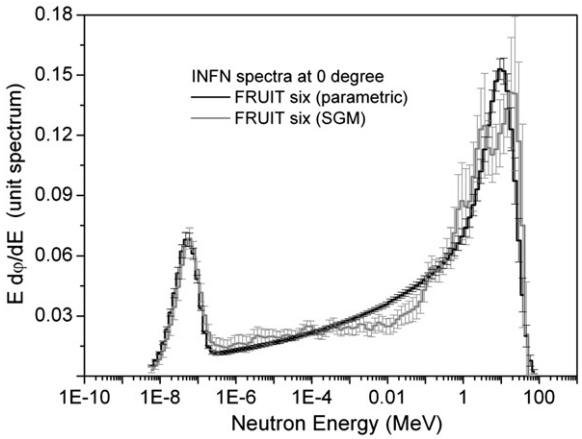

Fig. 5. Point A, INFN data: neutron spectrum unfolded with FRUIT ver. six using the SGM approach and the parametric approach. The spectra are normalized to the unit fluence (unit spectra) and in equi-lethargy representation.

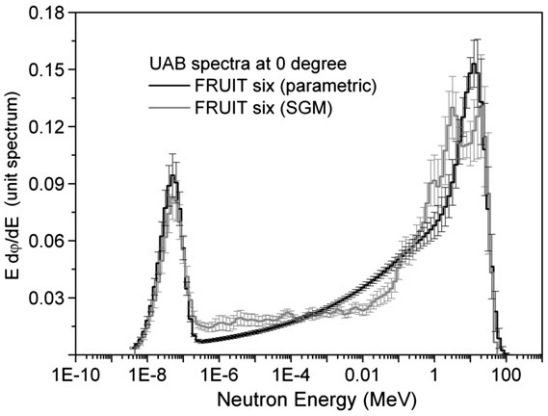

Fig. 6. Point A, UAB data: neutron spectrum unfolded with FRUIT ver. six, using the SGM approach and the parametric approach. The spectra are normalized to the unit fluence (unit spectra) and in equi-lethargy representation.

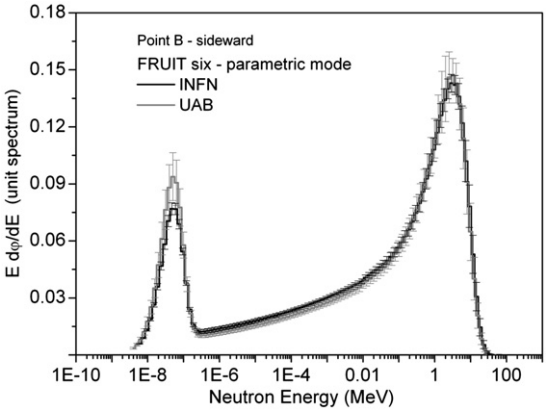

Fig. 7. Point B: neutron spectra unfolded with FRUIT ver. six, using the parametric approach. The spectra are normalized to the unit fluence (unit spectra) and in equi-lethargy representation.

Table 1
Spectrum integrated quantities for the spectra measured in points A and B by the UAB and INFN systems. The neutron fluence is normalized per one proton measured at the last current monitor before beam delivering.

Group	Unfolding method	Point	$h^*(10)$ pSv cm^2	Fluence (E − 8 cm^{-2})	Fluence fractions			
					$E<0.5$ eV	0.5 eV to 10 keV	10 keV to 10 MeV	$E>10$ MeV
UAB	Parametric	A	228 ± 7	18.0 ± 1.1	19%	18%	47%	16%
	SGM	A	235 ± 8	17.0 ± 1.1	17%	20%	49%	14%
	Parametric	B	189 ± 4	11.8 ± 0.6	19%	21%	58%	$<2\%$
INFN	Parametric	A	228 ± 4	18.8 ± 1.0	14%	23%	51%	12%
	SGM	A	248 ± 9	18.5 ± 1.0	14%	22%	50%	14%
	Parametric	B	189 ± 4	11.9 ± 0.6	17%	25%	58%	$<1\%$

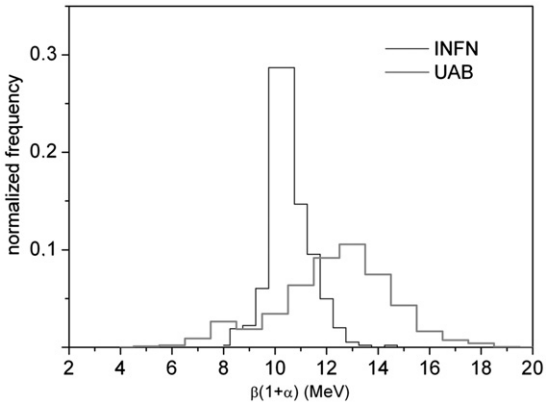

Fig. 8. Point A: probability distribution of the peak energy for INFN and UAB systems.

Fig. 7 shows the parametric spectra obtained from INFN and UAB data at point B.

Most of the considerations drawn in this section are underlined, from a quantitative point of view, in Table 1. Here the spectra obtained with different ERBSS and unfolding methods are compared in terms of: total fluence per unit incident proton, spectrum average fluence-to-ambient dose equivalent conversion coefficient, $h^*(10)$, and spectral indexes, i.e. fractions of fluence under the following energy intervals: $E<0.5$ eV (thermal), $0.5\text{ eV}<E<10$ keV (intermediate), and $10\text{ keV}<E<10$ MeV (fast) and $E>10$ MeV (high energy). From the values of the spectral indexes, it is clear that the spectrum in point A is harder than that in point B. This is confirmed by the values of $h^*(10)$.

The uncertainties of the neutron fluence have been estimated as the quadratic combination of the unfolding uncertainty (lower than $\pm4\%$ at 68% confidence level), the monitoring uncertainty ($\pm3\%$) and the uncertainty of the spectrometer calibration factor ($\pm2\%$).

A way to understand the importance of extended range spheres in determining the high-energy component of the spectrum, is the plot of Fig. 8, where the statistical distribution of the peak energy $\beta(\alpha+1)$ at point B is shown for INFN and UAB systems. These distributions are calculated on the basis of the α and β distributions reported by FRUIT (parametric option). The mean and s.d. of these distributions are 12.0 MeV with s.d. 2.2 MeV for UAB, and 10.2 MeV with s.d. 0.8 MeV for INFN.

The UAB extended range spheres (UAB-ERS-1 and UAB-ERS-2) have quite similar response functions, as shown in Fig. 3. The spheres INFN-ERS-1 and INFN-–ERS-2 are very similar to the correspondent UAB spheres, but the INFN system includes an additional sphere (INFN-ERS-3) having higher external diameter (12 in.) and lower diameter of the internal metal shell. This increases the degree of differentiation of the response functions and therefore the energy resolution, thus explaining the sharper probability distribution as shown in Fig. 8.

6. Conclusions

The neutron fields generated by a 62 MeV proton beam impinging a PMMA phantom were measured using the extended range Bonner Sphere Spectrometers of UAB and INFN. Two measurement points were established in the forward and sideward directions with respect to the direction of the incident protons. The INFN and UAB systems showed very coherent results, including the forward direction where an important high-energy component was expected. The FRUIT code, used in parametric or SGM modes independently, yielded accurate and reproducible results. An extensive uncertainty analysis of the problem was performed, including the estimation of the uncertainties of the spectra on a bin-per-bin basis. A simplified model made with MCNPX was useful, especially in case of the forward spectrum, to understand at which energy the neutrons could be produced. The simulated spectrum was used as default spectrum for the SGM method and helped in correctly selecting the spectrum parameterization in FRUIT.

Taking into account that the recent literature offers a limited number of measured neutron spectra at medical proton facilities, the results of this work may be of help for both medical physicist and radiation protection communities.

Acknowledgments

The beam time at the CATANA center of INFN-LNS proton beam was endorsed in the framework of the INFN project Micro-Si. The work was partially funded by the Spanish Ministerio de Ciencia e Innovación (MICINN) under Contract FIS2006-01843 and by the convention between INFN and MEC (Ministerio de Educación y Ciencia, Spain) INFN2008-09.

References

[1] W.D. Newhauser, J.D. Fontenot, A. Mahajan, D. Kornguth, M. Stovall, Y. Zheng, P.J. Taddei, D. Mirkovic, R. Mohan, J.D. Cox, S. Woo, Phys. Med. Biol. 54 (8) (2009) 2277.
[2] H. Nystrom, D.I. Thwaites, Radiother. Oncol. 86 (2008) 1.
[3] C. Domingo, M.J. Garcia-Fuste, E. Morales, K. Amgarou, J.A. Terron, J. Rosello, L. Brualla, L. Nunez, R. Colmenares, F. Gomez, G.H. Hartmann, F. Sanchez-Doblado, F. Fernandez, Radiat. Meas. 45 (10) (2010) 1391.
[4] Y. Zheng, J. Fontenot, P. Taddei, D. Mirkovic, W. Newhauser, Phys. Med. Biol. 53 (2008) 187.
[5] K. Tesch, Radiat. Prot. Dosim. 11 (3) (1985) 165.
[6] R.L. Bramlett, R.I. Ewing, T.W. Bonner, Nucl. Instr. and Meth. 9 (1960) 1.
[7] F.D. Brooks, H. Klein, Nucl. Instr. and Meth. A 476 (2002) 1.
[8] A.V. Alevra, D.J. Thomas, Radiat. Prot. Dosim. 107 (1–3) (2003) 37.
[9] M. Reginatto, Nucl. Instr. and Meth. A 480 (2002).

[10] M.B. Chadwick, et al., Nucl. Data Sheets 107 (2006) 2931.
[11] B. Wiegel, A.V. Alevra, Nucl. Instr. and Meth. A 476 (2002) 36.
[12] R. Bedogni, A. Esposito, J.M. Gómez-Ros, Radiat. Meas. 45 (2010) 1205.
[13] R. Bedogni, P. Ferrari, G. Gualdrini, A. Esposito, Radiat. Meas. 45 (2010) 1201.
[14] R. Bedogni, A. Esposito, A. Gentile, M. Angelone, G. Gualdrini, Radiat. Meas. 43 (2008) 1104.
[15] V. Lacoste, V. Gressier, J.-L. Pochat, F. Fernandez, M. Bakali, T. Bouassoule, Radiat. Prot. Dosim. 110 (1–4) (2004) 529.
[16] F. Fernández, T. Bouassoule, K. Amgarou, C. Domingo, M.J. Garcia, V. Lacoste, V. Gressier, H. Muller, Radiat. Prot. Dosim. 126 (1–4) (2007) 366.
[17] R. Bedogni, A. Esposito, C. Domingo, F. Fernández, M.J. Garcia, M. Angelone, Radiat. Prot. Dosim. 126 (1–4) (2007) 342.
[18] R. Bedogni, C. Domingo, A. Esposito, M. Chiti, M.J. García-Fusté, G. Lovestam, Nucl. Instr. and Meth. A 620 (2010) 391.
[19] A. Esposito, R. Bedogni, C. Domingo, M.J. García, K. Amgarou, Radiat. Meas. 45 (2010) 1522.
[20] R. Bedogni, C. Domingo, A. Esposito, F. Fernández, Nucl. Instr. and Meth. A 580 (2007) 1301.
[21] R. Bedogni, M. Pelliccioni, A. Esposito, Nucl. Instr. and Meth. A 615 (2010) 78.
[22] S. Yonai, N. Matsufuji, T. Kanai, Y. Matsui, K. Matsushita, Radiat. Meas. 45 (2010) 1369.
[23] B. Wiegel, S. Agosteo, R. Bedogni, M. Caresana, A. Esposito, G. Fehrenbacher, M. Ferrarini, E. Hohmann, C. Hranitzky, A. Kasper, S. Khurana, V. Mares, M. Reginatto, S. Rollet, W. Rühm, D. Schardt, M. Silari, G. Simmer, E. Weitzenegger, Radiat. Meas. 44 (2009) 673.
[24] G.A.P. Cirrone, S. Coco, G. Cuttone, P.A. Lojacono, R. Messina, IEEE Trans. Nucl. Sci. NS-51 (2004) 860.
[25] N. Givehchi, F. Marchetto, L.M. Valastro, A. Ansarinejad, A. Attili, M.A. Garella, S. Giordanengo, V. Monaco, J.P. Montero, R. Sacchi, A. Boriano, F. Bourhaleb, R. Cirio, A. La Rosa, A. Pecka, C. Peroni, G.A.P. Cirrone, G. Cuttone, M. Donetti, S. Iliescu, S. Pittera, L. Raffaele, Phys. Med. (in press), doi:10.1016/j.physletb.2003.10.071.
[26] L.S. Waters (Ed.), MCNPXTM Users Manual, ECI, Version 2.4.0, Los Alamos National Laboratory Report LA-CP-02-408, 2002.
[27] R. Bedogni, Ph.D. Thesis, Universidad Autonoma de Barcelona, Barcelona, Spain, 2006.
[28] M. Matzke, Radiat. Prot. Dosim. 107 (1–3) (2003) 155.
[29] M. Reginatto., Radiat. Meas. 45 (2010) 1323.
[30] R. Bedogni, Radiat. Prot. Dosim (in press) doi:10.1093/rpd/ncr238.